Influence of hydrogen absorption–desorption on structural properties of $Dy_{1-x}Mm_xCo_2$ alloys

2008 J. Phys.: Condens. Matter 20 255224

(http://iopscience.iop.org/0953-8984/20/25/255224)

J. Phys.: Condens. Matter **20** (2008) 255224 (8pp) doi:10.1088/0953-8984/20/25/255224

Influence of hydrogen absorption–desorption on structural properties of $Dy_{1-x}Mm_xCo_2$ alloys

G Srinivas[1,2], V Sankaranarayanan[2] and S Ramaprabhu[1,3]

[1] Alternative Energy Technology Laboratory, Department of Physics, Indian Institute of Technology Madras, Chennai-600 036, India
[2] Low Temperature Laboratory, Department of Physics, Indian Institute of Technology Madras, Chennai-600 036, India

E-mail: ramp@iitm.ac.in

Received 12 January 2008, in final form 11 April 2008
Published 21 May 2008
Online at stacks.iop.org/JPhysCM/20/255224

Abstract

The effect of hydrogen absorption–desorption on the structural properties of Laves phase $Dy_{1-x}Mm_xCo_2$ ($x = 0.1$, 0.3 and 0.5; Mm = mischmetal, a natural mixture of the light rare earth metals containing 50 wt% Ce, 35 wt% La, 8 wt% Pr, 5 wt% Nd and 1.5 wt% of other rare earth elements and 0.5 wt% Fe) alloys has been investigated by means of hydrogen absorption–desorption pressure-composition (PC) isotherms, kinetics of hydrogen absorption and powder x-ray diffraction (XRD). The PC isotherms and kinetics of hydrogen absorption have been studied in the pressure range 0.001–1 bar and temperature range 50–200 °C using Sieverts-type apparatus. The experimental results of the kinetic curves are interpreted using the Johnson–Mehl–Avrami (JMA) model and the reaction order and reaction rate have been determined. The α-, $(\alpha + \beta)$- and β-phase regions have been identified from the different slope regions of the PC isotherms and first-order type kinetic plots. The dependence of the reaction rate parameter upon hydriding pressure and temperature in the $(\alpha + \beta)$-phase region has been discussed. The effect of hydrogenation pressure, temperature and Mm concentration on the hydrogen-induced transformation from crystalline $Dy_{1-x}Mm_xCo_2$–H to amorphous $Dy_{1-x}Mm_xCo_2$–H and decomposition into crystalline (Dy, Mm)H_2 and Co have been discussed in detail. Further, the effect of dehydrogenation on the recovery of the crystalline Laves phase structure of $Dy_{1-x}Mm_xCo_2$ from its decomposed state is presented. This hydrogenation–disproportionation–desorption–recombination (HDDR) process can be conveniently used in powder metallurgy.

(Some figures in this article are in colour only in the electronic version)

1. Introduction

There is strong current interest in materials for reversible storage of hydrogen as a clean fuel [1]. Much attention has been focused on the hydrogen absorption and its influence on the structural, magnetic and electronic properties of intermetallic compounds [2–4]. A large number of these intermetallics, especially Laves phase compounds in which a rare earth element is one of the components, have been given much importance due to their easy hydride formation and unusual structural transformations due to hydrogen treatment at elevated temperatures and pressures [5–7].

There are a few investigations on the hydrogen absorption–desorption and thermodynamic properties of Laves phase RM_2 (R = rare earth; M = Mn, Fe, Co, Ni) compounds, because of their very low plateau pressures and complex hydrogen absorption and desorption properties [2, 8]. The RM_2-hydrides are mostly very stable in nature and relatively very little hydrogen can be released compared to that of absorbed hydrogen even when heated to 500 °C at

[3] Author to whom any correspondence should be addressed.

0.02 bar [8]. The hydriding–dehydriding properties can be tuned by partial replacement or alloying with different kinds of elements [2, 9–14]. Most of the hydrogen storage materials are multi-element alloys and a lot of effort has been made to optimize the materials for the best practical performance. However, the fundamental understanding of the mechanism and kinetics of the hydrogen absorption reaction in these materials is also considerably important. For example, the investigation of the kinetics of metal hydrides helps one to map the reaction mechanisms of hydrogen absorption and desorption. The reaction kinetics is greatly influenced by temperature and pressure but mostly the hydriding–dehydriding kinetics are investigated with the influence of temperature in order to determine the reaction rate and mechanism [15, 16]. A few of the investigations have also been carried on the effect of the initial hydrogen pressure of the system [17–20]. The hydriding reaction strongly depends on the hydrogen pressure of the system, when the hydriding pressure is not too high relative to the equilibrium pressure of the hydride [20].

It is important to study the stability of crystalline hydrides upon both the hydrogen absorption as well as desorption modes as a function of temperature and hydrogen pressure. A great deal of interest has been given to hydrogen-induced amorphization (HIA), i.e. the transformation from a crystalline to an amorphous phase by hydrogen absorption [21–26]. The formation of amorphous hydrides and their decomposition into constituent hydrides greatly depends on the hydrogenation temperature [27], the hydrogen pressure [28] and the type of rare earth or transition metal present in the host RM_2 alloy [5, 9, 13, 24, 29, 30]. However, there are a few investigations on the HIA and decomposition of the pseudobinary and ternary alloys, in which the occurrence of HIA mainly depends on the substitution of the third element in either of the sites of binary Laves phase RM_2 alloys [9, 13, 31, 32]. For example, the tendency for the occurrence of HIA in $HoCo_2$ drastically decreases when substituting Zr or Ti at the Ho site [9, 29]. The binary $ErMn_2$ does not exhibit any sign of amorphization but a small substitution of Co for Mn in $ErMn_2$ can make it possible to transform into an amorphous state [32].

In the present study, the hydrogen absorption and desorption properties of partial Mm substituted $DyCo_2$ have been investigated by pressure-composition (PC) isotherms and kinetics of hydrogen absorption. Mm is a natural mixture of rare earth elements, mostly consisting of Ce (30–52 wt%), La (13–25 wt%) Nd, Pr or Sm (13–57 wt%), with amounts depending on the place of origin [12, 33]. In this present study we have used the Indian mischmetal, which consists of 50 wt% Ce, 35 wt% La, 8 wt% Pr, 5 wt% Nd and 1.5 wt% of other rare earth elements and 0.5 wt% Fe [13]. Any variation in the composition of Mm would affect the results, thus a particular batch of Mm has been used in this study. Mm has been used mainly for economical reasons because mischmetal is obtained directly from the ore, without involving a costly rare earth separation [33]. The influence of the hydriding pressure and temperature on the absorption kinetics of activated samples has been studied and the dependence of rate constant in the two-phase region has been discussed. The effect of partial substitution of Mm, hydrogenation pressure and temperature and dehydrogenation on the hydrogen-induced structural transformations have been studied and the role of the alloying element, the amorphization conditions and mechanism are discussed on the basis of the observed experimental results.

2. Experimental details

The polycrystalline $Dy_{1-x}Mm_xCo_2$ (x = 0.1, 0.3, and 0.5) alloys were prepared by arc melting in an argon atmosphere from Co of 99.99% purity and Dy and Mm with a typical purity of 99.9% under a protective argon atmosphere. To ensure homogeneity, the alloys were inverted and remelted several times. An excess of 6 wt% of Dy and Mm were taken in order to prevent the formation of Co-rich phases. The ingots were sealed in an evacuated quartz tube and homogenized at 1123 K for four days. Hydrogen absorption–desorption PC isotherms and kinetics of hydrogen absorption in the pressure range 0.001–1 bar and temperature range 100–250 °C were performed using a homemade glass Sieverts apparatus. The change of the structure caused by the hydrogen-induced amorphization was examined by x-ray diffraction with monochromatized Cu Kα radiation. The x-ray diffraction (XRD) measurements were performed at room temperature by using an X'pert PRO, a PANalytical diffractometer with a step size of 0.05°. The high pressure hydrogenation at elevated temperatures was performed using stainless steel Sieverts apparatus. The exposure time of samples to given hydrogen pressure and temperature is restricted for about 1 h in each case. In order to avoid possible hydrogen desorption, the sample cell was cooled down to room temperature, then pressure was reduced to the atmospheric value. The samples were removed immediately from the sample cell and used for XRD measurements. The high temperature hydrogen desorption measurements were carried out by evacuating the system up to 10^{-5} mbar for at least 2 h for each specified sample temperature.

3. Results and discussion

3.1. Hydrogen absorption–desorption PC isotherms

The hydrogen absorption and desorption pressure-composition isotherms of $Dy_{0.9}Mm_{0.1}Co_2$ in the pressure range 0.001–1 bar at 150 and 200 °C are shown in figure 1. The closed and open symbols represent the absorption and desorption processes respectively. Each experimental data point in the plots represent equilibrium between hydrogen pressure in the system and hydrogen content in the alloy. On increasing hydrogen pressure, the interaction between the alloy and the hydrogen results in the system exhibiting three different phase regions, i.e. one with a low concentration phase of hydrogen-saturated alloy called the α-phase (the first sloping region), another with a high concentration hydride phase called the β-phase and a coexistence of these two (($\alpha + \beta$)-phase) phase regions, called the plateau region. The evidence for

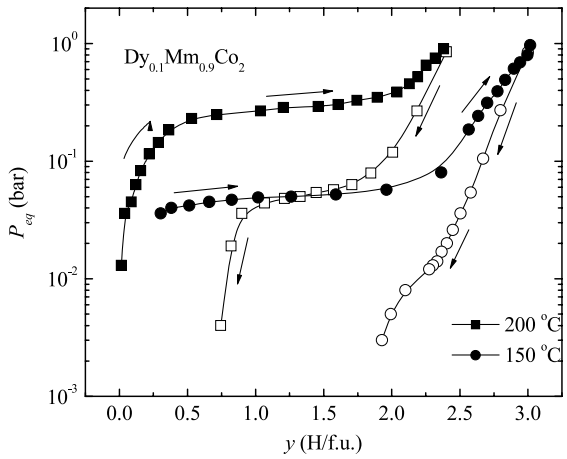

Figure 1. Hydrogen absorption–desorption pressure-composition isotherms of $Dy_{0.9}Mm_{0.1}Co_2$ at 150 and 200 °C in the pressure range of 0.001–1 bar; closed and open data points represent the hydrogen absorption and desorption processes respectively.

the existence of α-, $(\alpha + \beta)$- and β-phases can also be found in the kinetics of hydrogen absorption (section 3.2) or desorption [34, 35] and structural analysis by powder XRD of hydrides (section 3.3) of isostructural alloys [3, 36, 37]. In the kinetics of hydrogen absorption, the reaction rate proceeds differently in different phase regions. The different hydride phases in the $Ho_{1-x}Mm_xCo_2$–H_y system were distinguished by differences in the lattice constants [3]. α-phase has a lattice parameter close to that of the unhydrogenated $Ho_{1-x}Mm_xCo_2$ alloys. The growth of the β-phase results in a large lattice expansion. In the intermediate hydrogen concentrations, i.e. $(\alpha + \beta)$-phase region, all the XRD lines split into two sets of identical lines, representing the coexistence of the two hydride phases. This coexistence of two hydride phases was further evidenced by perturbed angular correlation (PAC) and Mossbauer measurements of isostructural Laves phase RM_2–H_y [36–38]. The hydrogen desorption PC isotherms of $Dy_{0.9}Mm_{0.1}Co_2$ at 200 °C show three different phase regions and reveal that the entire amount of absorbed hydrogen cannot be released. Further, the desorption plateau pressure appears at far lower pressures when compared to that of the absorption plateau at the same temperature, which will exhibit large hysteresis. The cause of hysteresis is mainly thought to be due to lattice expansion on hydriding. The formation of the hydride phase induces large strain and causes an irreversible plastic deformation in the alloy matrix when desorption of a small amount of hydrogen primarily relaxes the residual forces so that the phase is no longer under stress. Therefore, desorption should occur at a lower critical transition pressure. Because of strain sensitivity, the amount and size of impurities as well as the processing history have considerable effect on the absorption pressure plateau. The disappearance of the desorption plateau and negligible desorption capacity of hydrogen is found at 150 °C. PC isotherms show that the maximum hydrogen absorption capacity (H/f.u.) increases with the decrease in temperature and it appears in the reverse trend for desorption capacity. This hydride phase is quite stable, so that absorbed hydrogen cannot be fully released under the present experimental conditions [39].

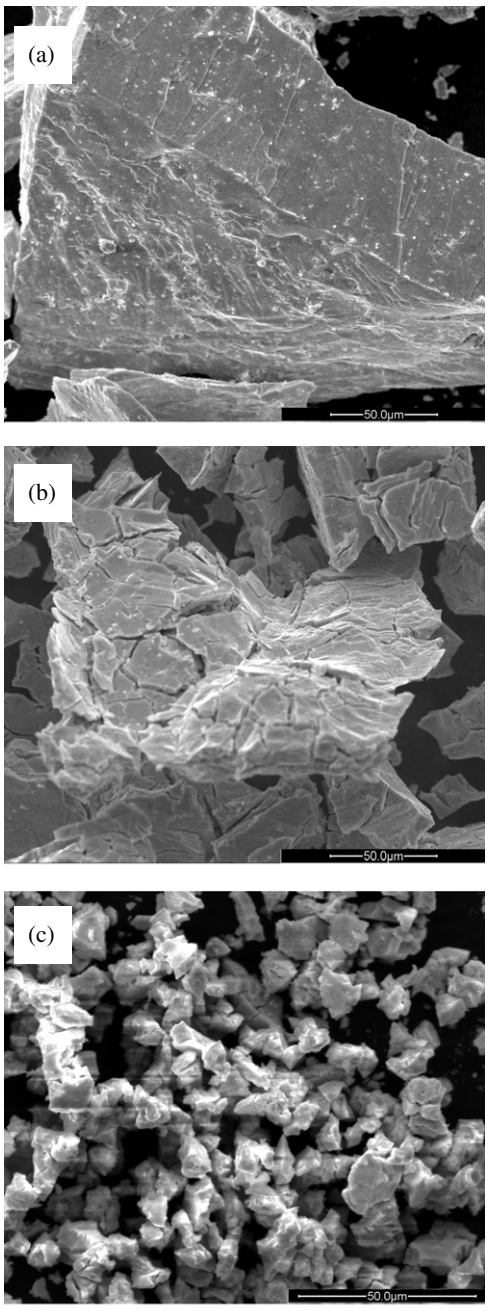

Figure 2. SEM images of $Dy_{0.9}Mm_{0.1}Co_2$-hydrides; (a) before hydrogenation (ingot), (b) after first cycle of hydrogenation and (c) after fourth cycle of hydrogenation.

3.2. Kinetics of hydrogen absorption

The pressure and temperature dependent kinetics of hydrogen absorption have been studied for the activated $Dy_{0.9}Mm_{0.1}Co_2$ alloys. The activation process consists of a series of absorption and desorption cycles. During activation, the change in surface morphology of alloys has been studied by scanning electron microscopy (SEM). Figures 2(a)–(c) show the SEM images of $Dy_{0.9}Mm_{0.1}Co_2$ and $Dy_{0.9}Mm_{0.1}Co_2$–H for the first and fourth

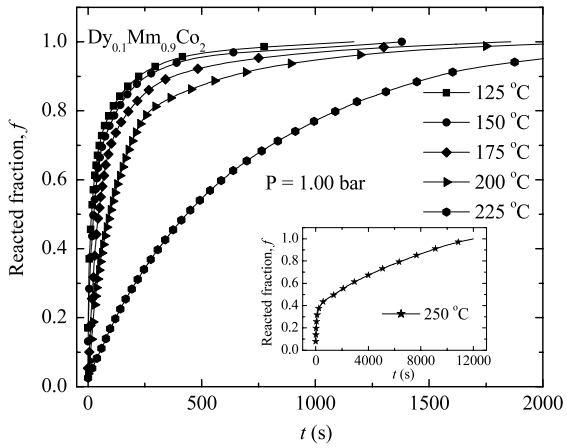

Figure 3. Temperature dependent hydrogen absorption kinetic plots of activated $Dy_{0.9}Mm_{0.1}Co_2$ with initial applied hydrogen pressure of 1 bar; inset shows the kinetic plot at 250 °C.

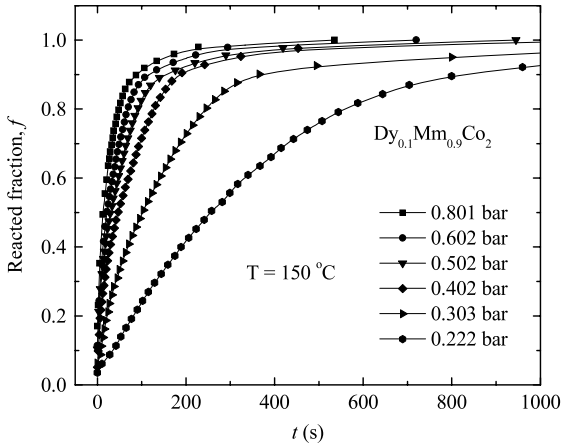

Figure 4. Pressure dependent hydrogen absorption kinetic plots of activated $Dy_{0.9}Mm_{0.1}Co_2$ at 150 °C.

hydrogen cycles. The vigorous breakage of the alloy particles can be seen by the appearance of a large number of microcracks just after a complete initial hydrogen absorption step. The formation of fine powders can be seen by further repeating the hydrogenation cycles. The large volume expansion during hydride formation (observed by XRD, section 3.3) and the brittle nature of RCo_2 alloys lead to the formation of a fine powder with fresh surfaces. This leads to the instantaneous and homogeneous hydrogen absorption by all the alloy particles. Such activated hydrogen absorption kinetic curves plotted as reacted fraction, f, versus time are shown in figure 3 as a function of temperature. The reacted fraction, f, is obtained from the ratio

$$f(t) = (P - P(t))/(P - P\infty) \tag{1}$$

where P is the applied pressure of the reaction. $P(t)$ and $P\infty$ are the pressures at time t and final equilibrium, respectively. Figure 4 shows the influence of the applied hydrogen pressure on the hydrogen absorption kinetics of the activated $Dy_{0.9}Mm_{0.1}Co_2$ alloys. It is clear from the qualitative behavior of the kinetic plots, that the reaction starts immediately without an induction period. In addition, with decreasing applied hydrogen pressure or on increasing sample temperature the kinetics appears to be slower and takes longer time to complete the reaction, i.e. the reaction rate is decreasing. This can be considered as being primarily due to the decrease of the driving force $(P - P_{eq})$ for hydrogen absorption, with decreasing pressure or increasing temperature. The absorption pressure-composition isotherms (figure 1) reveal the existence of phase boundaries and three-phase regions i.e. the α-phase, the β-phase and a coexistence of these two ($(\alpha + \beta)$-phase) phase region. In general, the hydrogen absorption proceeds differently in these different phase regions. In order to get the proper reaction rate constants, reaction order (growth dimensionality of the hydride phase) and reaction mechanism in different phase regions, these kinetic plots are further analyzed by using a conventional Johnson–Mehl–Avrami (JMA) type nucleation and growth

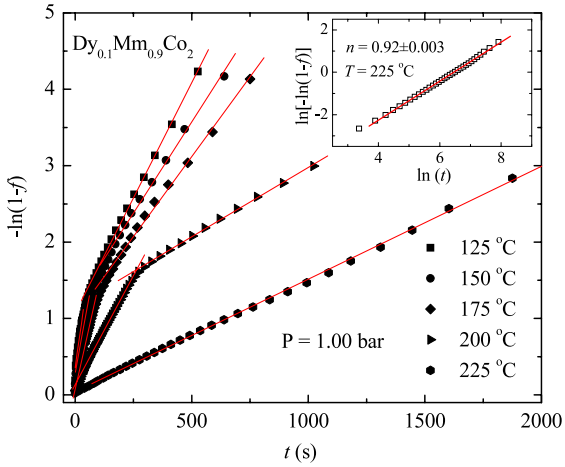

Figure 5. Temperature dependent hydrogen absorption first-order type kinetic plots of $Dy_{0.9}Mm_{0.1}Co_2$ alloy at an applied initial pressure of 1 bar; inset shows the $\ln[-\ln(1-f)]$ versus $\ln(t)$ plot at 225 °C and 1.00 bar.

theory [40–42], where the reacted fraction of alloy hydride, $f(t)$, is given as a function of time t, by

$$f(t) = 1 - \exp(-kt^n). \tag{2}$$

Here k represents the nucleation and growth rates of the reaction kinetics, the exponent, n, called the Avrami exponent, provides information about the dimensionality or order of the growing hydride phase or transformation. Rearranging equation (2), one gets

$$\ln[-\ln(1 - f)] = n \ln t + \ln k. \tag{3}$$

Equation (3) indicates that, at a given temperature and pressure, a plot of $\ln[-\ln(1 - f)]$ versus $\ln(t)$ is expected to be linear. The slope and intercept of a linear interpolation of the typical master plots, $\ln[-\ln(1 - f)]$ versus $\ln(t)$, yields values of n and k respectively. For example, the insets of figures 5 and 6 show $\ln[-\ln(1 - f)]$ versus $\ln(t)$ plots for $Dy_{0.9}Mm_{0.1}Co_2$–H at 225 °C for an applied pressure of 1 bar

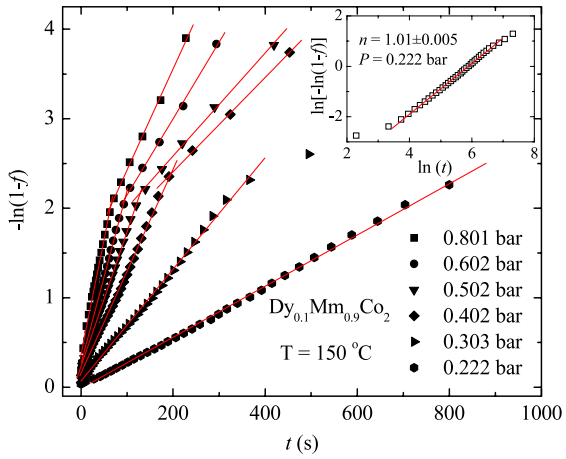

Figure 6. Pressure dependent hydrogen absorption first-order type kinetic plots of $Dy_{0.9}Mm_{0.1}Co_2$ alloy at 150 °C; inset shows the $\ln[-\ln(1-f)]$ versus $\ln(t)$ plot at 0.222 bar and 150 °C.

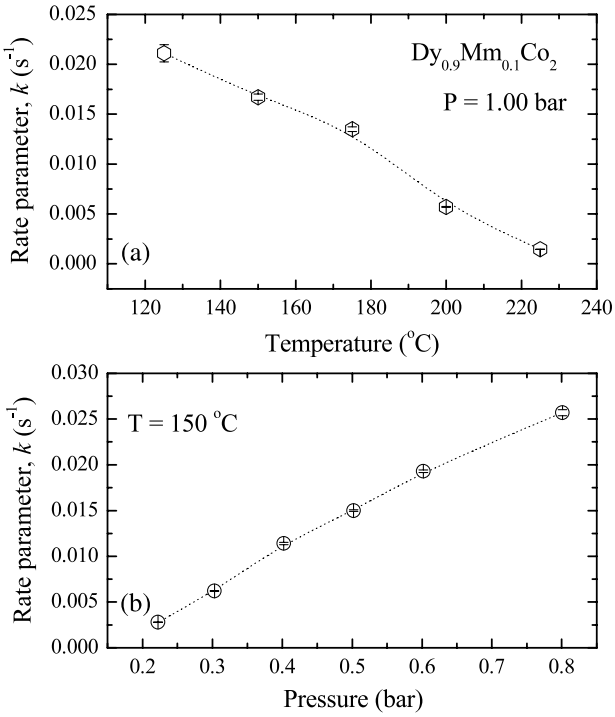

Figure 7. Variation of hydrogen absorption rate parameter for $Dy_{0.9}Mm_{0.1}Co_2$ in the $(\alpha+\beta)$-phase region as a function of (a) temperature at an initial pressure of 1 bar and (b) pressure at 150 °C.

and at 150 °C for an applied pressure of 0.222 bar respectively. A best linear fit of the experimental data in the $(\alpha+\beta)$-phase region gives the average values of n very close to 1 ($n = 1 \pm 0.1$). Thus the reaction order indicates that the hydriding reactions are of first-order type, i.e. that the growth of the hydride phase is planar. The sample temperature and applied system pressure dependent first-order type kinetic plots ($-\ln(1-f)$ versus t) of figures 3 and 4 are shown in figures 5 and 6 respectively. These plots clearly demonstrate, in almost all the kinetic plots, the existence of two different linear segments, which extend in a certain range rather than being linear over the entire reaction range. These plots involve a phase transformation; the first straight-line segment represents the $(\alpha+\beta)$-phase region and the second straight-line segment represents the β-phase region [15, 16, 34, 35, 43, 44]. There is no evidence of the α-phase region due to the fast hydriding reaction. At higher temperatures there is no clear evidence of the β-phase formation in these experimental conditions, due to the higher equilibrium plateau pressures P_{eq}. The applied pressure and sample temperature dependence of the hydrogen absorption rate constants in the $(\alpha+\beta)$-phase region are shown in figure 7. The rate constants increase almost linearly with increasing hydriding pressure and follow the opposite trend with increasing temperature. In most of the cases, it has been found that the apparent rate constant is independent of applied pressure and further increases with increasing temperature (i.e. thermally activated behavior), when hydrogenated at higher pressures than their plateau pressures [15, 16]. However, the rate constant largely depends on the driving force, $P_d = P - P_{eq}$, when the applied pressure is not high relative to that of the equilibrium plateau pressure. When the hydriding kinetics is carried out at near equilibrium pressures, the increase in temperature would largely reduce the driving force $(P - P_{eq})$, since the hydrogen equilibrium pressure P_{eq} increases with the increase in temperature (figure 1). The reaction rate is more sensitive in the case of low initial $(P - P_{eq})$ than that of high initial $(P - P_{eq})$. As a result, the reaction rate is slower at higher temperatures or lower hydriding pressures [17, 34, 35, 45–47]. Mg_2Ni–H [17] and U–H [20] systems show the same trend when kinetics is carried out at near equilibrium pressures.

3.3. Hydrogen-induced amorphization

The XRD patterns of homogenized $Dy_{1-x}Mm_xCo_2$ ($x = 0.1$, 0.3 and 0.5) alloys (e.g. figures 8(a) and 9(a)) indicate the cubic Laves phase with the $MgCu_2$-type structure (space group $Fd\bar{3}m$). The lattice parameter ($a = 7.195 \pm 0.001$, 7.208 ± 0.001 and 7.221 ± 0.003 for $x = 0.1$, 0.3 and 0.5 respectively) increases linearly with increasing Mm concentration, which is ascribed to the larger radius of the Mm than that of Dy, since the mischmetal is an ore of lighter rare earths, which have larger radii than the heavier rare earth Dy. Figure 8 shows the XRD patterns of $Dy_{0.9}Mm_{0.1}Co_2$–H, subjected to various hydrogenation pressures and temperatures. In the α-phase region, XRD of $Dy_{0.9}Mm_{0.1}Co_2$ looks very similar to the parent alloys and indicates a negligible change in the lattice parameters. In the β-phase region the hydrides retain their cubic C15 host lattice structure and a large shift of diffraction lines towards the lower angle side represents the substantial lattice expansion maximum of about 25 vol%. However, when hydrogenated at higher temperatures and pressures (figure 8(f)) the complete disappearance of diffraction lines indicates the amorphous nature of $Dy_{0.9}Mm_{0.1}Co_2$–H. In order to understand much more clearly the effect of the hydrogenation temperature and pressure on HIA, figures 9 and 10 are shown respectively for the $Dy_{0.5}Mm_{0.5}Co_2$–H system. Upon increasing hydrogenation temperature or pressure, XRD shows the complete disappearance and appearance of new types of diffraction lines. The new weak broad Bragg peaks from the

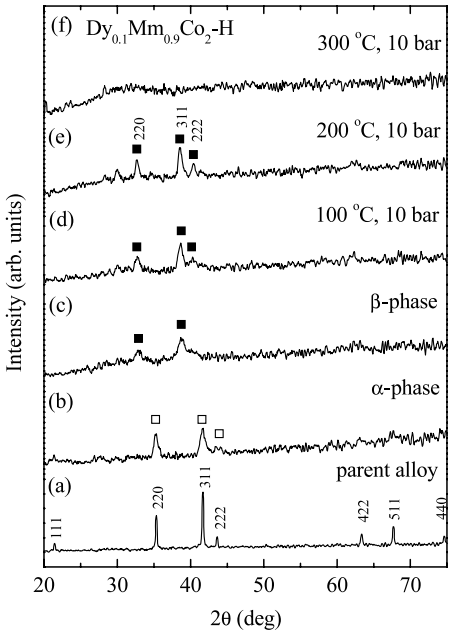

Figure 8. XRD patterns of $Dy_{0.9}Mm_{0.1}Co_2$ alloy hydrides, hydrogenated at different pressures and temperatures.

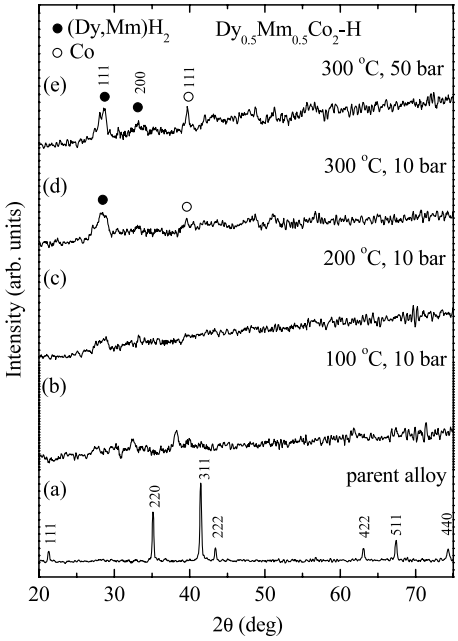

Figure 9. XRD patterns of $Dy_{0.5}Mm_{0.5}Co_2$ alloy hydrides, hydrogenated at different temperatures.

amorphous phase at elevated hydrogenation temperature or pressure are identified as fcc REH_2 (RE = Dy + Mm) and Co. Therefore, this indicates the decomposition of the amorphous alloy into REH_2 and Co. The comparison of XRD patterns of $Dy_{1-x}Mm_xCo_2$–H ($x = 0.1$, 0.3 and 0.5; hydrogenated at 10 bar and 300 °C) (figure 11) indicates that the amorphization and decomposition occurs more easily with increasing Mm substitution. In accordance with the previous investigations, the new broad XRD Bragg peaks in the decomposed state confirm the nanocrystalline nature of REH_2 and Co [48, 49].

The hydrogen pressure and temperature plays an important role in the hydrogen-induced transformation from the well crystalline state to amorphization. It is proposed that the C15 AB_2 Laves compounds can amorphize upon hydrogen absorption, when the atomic size ratio of the rare earth (A atom) and transition metal (B atom) is larger than 1.37 (i.e. $R_A/R_B > 1.37$) [5, 26]. In the Laves phase RCo_2 family, the amorphization temperature and the critical pressure of HIA as well as the decomposition temperature of the corresponding amorphous hydrides are found to decrease with decreasing atomic number of R. Thus the alloy hydrides containing lighter rare earths (e.g. La, Ce and Pr) more easily get amorphized than those heavier rare earth elements [5, 26, 50]. Since Mm is a mixture of light rare earths, the occurrence of HIA and decomposition into stable constituent hydrides take place at lower hydriding pressures and temperatures with increasing Mm substitution. Further, $Dy_{1-x}Mm_xCo_2$ alloys amorphize and decompose easily at lower hydriding pressures and temperatures when compared with the amorphization results of $Ho_{1-x}Mm_xCo_2$ [13]. It is mainly believed to be due to the increase in the atomic size ratio (i.e. $R_{Dy}/R_{Co} > R_{Ho}/R_{Co}$) and decrease in atomic number of Dy. In addition, the amorphization in $Dy_{1-x}Mm_xCo_2$–H can be explained based on the thermodynamic and kinetic aspects of the C15

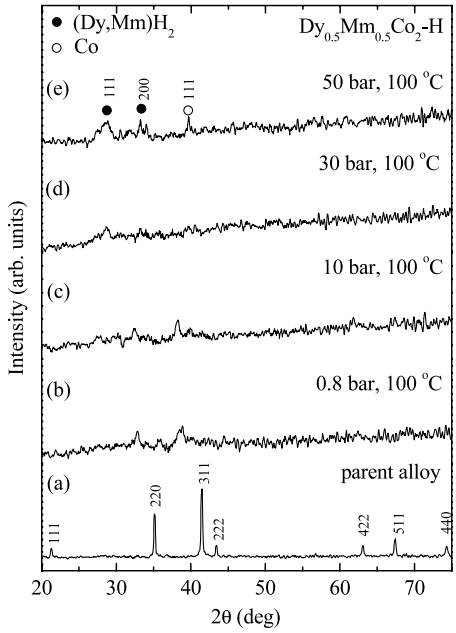

Figure 10. XRD patterns of $Dy_{0.5}Mm_{0.5}Co_2$ alloy hydrides, hydrogenated at different pressures.

Laves phase RM_2–H. It demonstrates that the enthalpy of amorphous RM_2–H is lower than that of crystalline RM_2–H, because the latter transforms to the former exothermically. The enthalpy difference can be explained on the basis of the environmental difference of hydrogen atoms in amorphous and crystalline RM_2–H. According to the geometrical constraints, the hydrogen atoms in the C15 Laves phases RM_2–H occupy the tetrahedral sites surrounded by 2R2M or 1R3M [51]. However, in the case of amorphous RM_2–H the hydrogen atoms can occupy the tetrahedral sites surrounded by 4R,

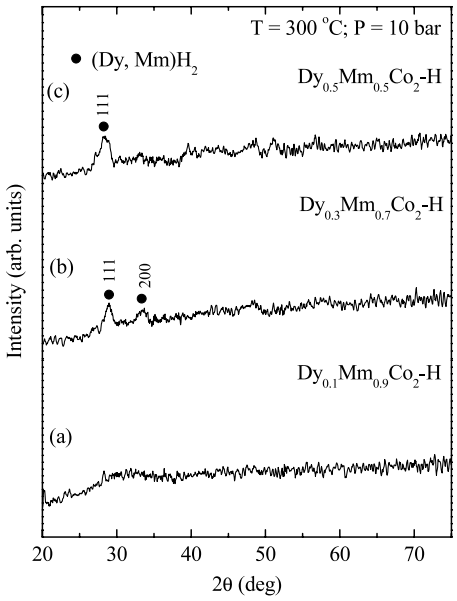

Figure 11. XRD patterns of $Dy_{1-x}Mm_xCo_2$ ($x = 0.1$, 0.3 and 0.5) alloy hydrides, hydrogenated at 300 °C and 10 bar.

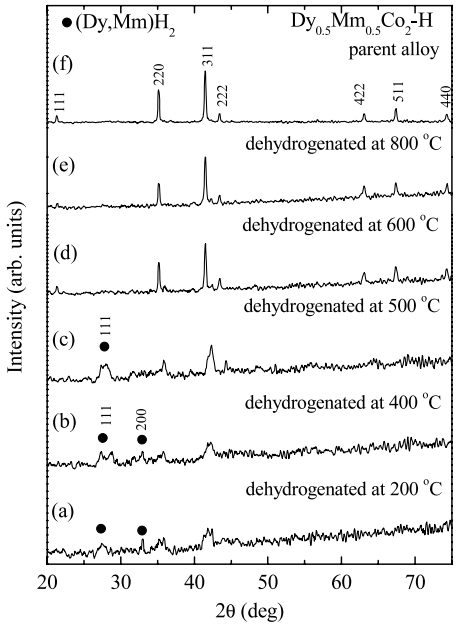

Figure 12. XRD patterns of $Dy_{0.5}Mm_{0.5}Co_2$ alloy hydrides, dehydrogenated at different temperatures.

3R1M, 2R2M and 1R3M [52]. Since rare earths have large negative heat of mixing, the hydrogen atoms tend to surround themselves by R atoms [26] and therefore the hydrogen atoms in the amorphous phases are much more strongly bound than those in the corresponding crystalline phases. Therefore, the amorphous hydride phase is relatively more stable than the crystalline hydride phase. When the crystalline RM_2 alloys are hydrogenated at higher temperatures, where the metal atoms can move easily, rearrangement of the metal atoms can occur to reduce the total free energy of the alloy and this leads to the HIA [27]. Since the diffusion rates of metallic atoms are very low at lower temperatures and below critical pressures, the hydrogen absorbed system retains its crystalline state without any change in the structure. That is why the formation of the amorphous phase is suppressed for a kinetic reason at low temperatures and pressures. However, when hydrogenated further at higher temperatures and pressures, where the metal atoms can move much more easily, the amorphous phase is no longer stable and so RH_2 precipitates in the amorphous phase or the amorphous RM_2–H phase decomposes into the more stable phases RH_2 (RH_3) and M. The precipitation of RH_2 requires the long-range diffusion of R atoms. Therefore, the short-range order in the amorphous phase is likely to depend on the temperature and hydrogen pressure [53].

The effect of hydrogen desorption on the structural transformation of $Dy_{0.5}Mm_{0.5}Co_2$ is given in figure 12. The disproportionated $Dy_{0.5}Mm_{0.5}Co_2$ alloy hydride is heated in the temperature range 200–800 °C in a vacuum and XRD has been carried out for the determination of the nature of the structure due to the hydrogen desorption. When partial hydrogen is released from the hydride in the temperature range 200–500 °C, several low-intensity peaks corresponding to the C15 type Laves phase and REH_2 were observed and the relative intensity of the C15 structure increased. As the complete hydrogen desorption temperature is above 500 °C for the isostructural $Ho_{1-x}A_xCo_2$–H (A = Mm, Ti) system observed from the thermogravimetric analysis (TGA) [14, 39], one can see that the recombination of products of partly decomposed $Dy_{0.5}Mm_{0.5}Co_2$ alloy is completed with recovery of the C15 type Laves phase due to the almost complete hydrogen release at 600 °C. After heating to a temperature of 800 °C, one can observe a similar structure to that of the parent alloy with a negligible change in lattice parameters. It is also observed in the case of the RFe_2–H system, where the increase in hydrogenation temperature and pressure causes transformation from crystalline hydride (RFe_2–H) to the amorphous state and decomposition to R–H and fcc-Fe phases. While after subsequent degassing of hydrogen from the sample by vacuum treatment at higher temperatures, the disproportionated phases recombine, forming the initial C15 structure RFe_2 compound [54]. This hydrogenation–disproportionation–desorption–recombination (HDDR) process is frequently used for the preparation of high coercive hard magnetic rare earth alloys, e.g. Nd–Fe–B, Sm–Fe–N [55].

4. Summary

During the hydrogen absorption process, $Dy_{1-x}Mm_xCo_2$ ($x = 0.1$, 0.3 and 0.5) alloys exhibit three different phase regions: the α-phase, β-phase and a coexistence of these two ($(\alpha + \beta)$-phase). The hydrogen absorption kinetics follows a first-order type reaction. Reaction rate follows inverse temperature behavior due to a decrease in the driving force ($P - P_{eq}$) with increase in temperature. At lower hydriding pressure and temperatures, $Dy_{1-x}Mm_xCo_2$-hydrides retain their Laves C15 structure with a volume expansion of about 25%. However, with increasing hydriding pressure and temperature, the crystalline $Dy_{1-x}Mm_xCo_2$–H changes to amorphous $Dy_{1-x}Mm_xCo_2$–H and the resultant amorphous

$Dy_{1-x}Mm_xCo_2$–H decomposes into crystalline fcc (Dy, Mm) H_2 and Co. The conditions for HIA strongly depend on the Mm concentration. The hydrogen desorption at elevated temperatures in vacuum leads to the recovery of the parental alloy C15 structure from the decomposed state (HDDR) and this property can be conveniently used in powder metallurgy.

Acknowledgment

The authors thank IITM, Chennai for financial support.

References

[1] Schlapbach L and Zuttel A 2001 *Nature* **414** 353
[2] Schlapbach L 1988 *Hydrogen in Intermetallic Compounds I* (*Topics in Applied Physics vol 63*) (Berlin: Springer)
[3] Srinivas G, Sankaranarayanan V and Ramaprabhu S 2007 *J. Appl. Phys.* **102** 063706
[4] Srinivas G, Sankaranarayanan V and Ramaprabhu S 2007 *Solid State Sci.* **9** 973
[5] Aoki K and Masumoto T 1993 *J. Alloys Compounds* **194** 251
[6] Chio M D, Livraghi S and Baricco M 2006 *J. Alloys Compounds* **426** 180
[7] Zavaliy I Yu, Cerny R, Verbetsky V N, Denys R V and Riabov A B 2003 *J. Alloys Compounds* **358** 146
[8] Jacob I and Shaltiel D 1979 *J. Less-Common Met.* **65** 117
[9] Ramesh R and Rama Rao K V S 1993 *J. Alloys Compounds* **191** 101
[10] Ozaki T, Yang H B, Iwaki T, Tanase S, Sakai T, Fukunaga H, Matsumoto N, Katayama Y, Tanaka T, Kishimoto T and Kuzuhara M 2006 *J. Alloys Compounds* **408–412** 294
[11] Yu X B, Dou T, Wu Z, Xia B J and Shen J 2006 *Nanotechnology* **17** 268
[12] Kleperis J, Wojcik G, Czerwinski A, Skowronski J, Kopczyk M and Beltowska-Brzezinska M 2001 *J. Solid State Electrochem.* **5** 229
[13] Srinivas G, Sankaranarayanan V and Ramaprabhu S 2007 *J. Phys. D: Appl. Phys.* **40** 1183
[14] Srinivas G, Sankaranarayanan V and Ramaprabhu S 2008 *Mater. Sci. Eng.* A **472** 293
[15] Mani N and Ramaprabhu S 2005 *Int. J. Hydrogen Energy* **30** 53
[16] Kandavel M and Ramaprabhu S 2003 *J. Phys.: Condens. Matter* **15** 7501
[17] Song M Y, Pezart M, Darriet B and Hagemuller P 1985 *J. Solid State Chem.* **56** 191
[18] Li Q, Jiang L-J, Chou K-C, Lin Q, Zhan F, Xu K-D, Lu X-G and Zhang J-Y 2005 *J. Alloys Compounds* **399** 101
[19] Bereznitsky M, Jacob I, Bloch J and Mintz M H 2004 *J. Alloys Compounds* **363** 208
[20] Bloch J 2003 *J. Alloys Compounds* **361** 130
[21] Aoki K, Li H-W, Dilixiati M and Ishikawa K 2007 *Mater. Sci. Eng.* A **449–451** 2
[22] Aoki K, Li H-W and Ishikawa K 2005 *J. Alloys Compounds* **404–406** 559
[23] Li X G, Chiba A, Aoki K and Masumoto T 1997 *J. Alloys Compounds* **255** 253
[24] Aoki K and Masumoto T 1995 *J. Alloys Compounds* **231** 20
[25] Kim Y-G and Lee J-Y 1992 *J. Alloys Compounds* **187** 1
[26] Aoki K, Li X-G and Masumoto T 1992 *Acta Metall. Mater.* **40** 1717
[27] Aoki K, Li X-G, Hirata T and Masumoto T 1992 *Appl. Phys. Lett.* **61** 2422
[28] Ishikawa K, Ogasawara N and Aoki K 2005 *J. Alloys Compounds* **404–406** 599
[29] Srinivas G, Sankaranarayanan V and Ramaprabhu S 2008 *J. Alloys Compounds* **458** 574
[30] Aoki K, Li X-G, Hirata T, Matsubara E, Waseda Y and Masumoto T 1993 *Acta Metall. Mater.* **41** 1523
[31] Kim Y-G and Lee J-Y 1993 *J. Alloys Compounds* **191** 243
[32] Kim Y-G, Chung U-I and Lee J-Y 1992 *Acta Metall. Mater.* **40** 1497
[33] Palmer P E, Burkholder H R, Beaudry B J and Gschneidner K A Jr 1982 *J. Less-Common Met.* **87** 135
[34] Sinha V K, Pourarian F and Wallace W E 1982 *J. Less-Common Met.* **87** 283
[35] Srinivas G, Sankaranarayanan V and Ramaprabhu S 2008 *J. Alloys Compounds* **448** 159
[36] Saxce T D, Berthier Y and Fruchart D 1985 *J. Less-Common Met.* **107** 35
[37] Zukrowski J, Strecker M, Wortmann G, Przewoznik J and Krop K 1997 *J. Alloys Compounds* **261** 47
[38] Van Eek S M and Forker M 2002 *Phys. Rev.* B **65** 174307
[39] Srinivas G, Sankaranarayanan V and Ramaprabhu S 2007 *Int. J. Hydrog. Energy* **32** 2480
[40] Avrami M 1939 *J. Chem. Phys.* **7** 1103
[41] Karty A, Grunzweig-Genossar J and Rudman P S 1979 *J. Appl. Phys.* **50** 7200
[42] Kenneth Kelton F 1997 *Mater. Sci. Eng.* A **226–228** 142
[43] Zhang W, Cimato J and Goudy A J 1993 *J. Alloys Compounds* **201** 175
[44] Clay K R, Goudy A J, Schweibenz R G and Zarynow A 1990 *J. Less-Common Met.* **166** 153
[45] Srinivas G, Sankaranarayanan V and Ramaprabhu S 2007 *J. Phys. Chem. Solids* at press (Available online 28 November 2007)
[46] Wang X-L and Suda S 1992 *Int. J. Hydrog. Energy* **17** 139
[47] Lee J-Y, Byun S M, Park C N and Park J K 1982 *J. Less-Common Met.* **87** 149
[48] Kawahara K, Li X-G, Ishikawa K, Suzuki K and Aoki K 2001 *Scr. Mater.* **44** 2019
[49] Yermakov A Y, Zajkov N K, Mushnikov N V, Gaviko V S, Serikov V V and Kleinerman N M 1999 *Nanostruct. Mater.* **12** 797
[50] Paul-Boncour V, Lartigue C, Percheron-Guegan A, Achard J C and Pannetier J 1988 *J. Less-Common Met.* **143** 301
[51] Ivey D G and Northwood D O 1986 *J. Less-Common Met.* **115** 23
[52] Matsuura M, Fukamichi K, Komatsu H, Aoki K, Masurnoto T and Suzuki K 1988 *Mater. Sci. Eng.* **97** 223
[53] Mushnikov N V, Goto T, Gaviko V S and Zajkov N K 1999 *J. Alloys Compounds* **292** 51
[54] Zajkov N K, Mushnikov N V, Gaviko V S and Yermakov A Ye 1997 *Int. J. Hydrog. Energy* **22** 249
[55] Takeshita T 1993 *J. Alloys Compounds* **193** 231